European Journal of Soil Science, June 1995, **46**, 169–177

Measuring the millimetre-scale oxygen diffusivity in soil using microelectrodes

C. RAPPOLDT*
Department of Theoretical Production Ecology, Agricultural University, P.O. Box 430, 6700 AK Wageningen, The Netherlands

Summary

The diffusivity of oxygen in soil was measured by periodically changing the gas above a soil core from nitrogen to air and *vice versa*. The concentration wave was measured as a function of depth with an oxygen electrode. For different Fourier components in the signal, phase shifts were calculated. The diffusivity follows from the increase of the phase shift with depth. Phase shifts are more suitable than signal amplitudes for the derivation of diffusivity. They are also easier to measure and do not require electrode calibration.

For a clay soil with an air-filled porosity of about 0.05 $m^3\ m^{-3}$ a local diffusivity of 0.9×10^{-9} $m^2\ s^{-1}$ was measured. This is several orders of magnitude smaller than macroscopic values for entire core samples of the same soil type. This low value can be explained by the presence of locally water-saturated clay.

Introduction

Currie (1961) pointed out that anoxic zones may occur in a generally well aerated soil. That will be the case when oxygen transport largely takes place through inter-aggregate pores. Inside the soil aggregates oxygen transport may be too small to maintain oxic conditions everywhere.

A more general way of expressing this is that the oxygen diffusion coefficient depends on the scale on which it is measured. On a macroscopic scale, the diffusion coefficient is largely determined by the air-filled macropores. On a millimetre scale, inside soil aggregates for instance, the situation may be very different. Most pores may be water filled, leading to much lower oxygen diffusion and possibly to local anaerobiosis. In this paper a method is described for measuring the diffusivity of oxygen on a millimetre scale. The method is based on a phenomenon which is well known from heat transport. A periodic change of the oxygen concentration is applied to the surface of a soil sample. This leads to periodicity in the signal of an oxygen electrode at a few millimetres from the surface. The amplitude of this concentration wave decreases with depth while the phase shift increases. It is shown that the diffusivity can be best obtained from phase shifts.

The theoretical basis of the method is first discussed, and experimental details are given. Test results for oxygen diffusion in water are also presented. Then results are given for a clay soil. These demonstrate the existence of water-saturated zones with a size of several millimetres. Table 1 explains the symbols used.

Received 23 November 1993; revised version accepted 10 January 1995
*Present address: Institute for Agrobiology and Soil Fertility Research, P.O. Box 129, 9750 AC Haren, The Netherlands.

Method

First, the diffusivity of oxygen in soil is defined. Then, a homogenous soil is considered which is exposed at its surface to a sinusoidal concentration wave. The wave amplitude decreases exponentially with depth and the phase shift increases linearly. In principle, a diffusivity can be obtained from both measured wave amplitudes and measured phase shifts.

Two problems remain. The first is that air-filled macropores may cause deviations from the theory for a plane surface. Numerical calculations indicate that these deviations are smaller for phase shifts than for wave amplitudes. The second problem is a practical one. Switching between air and nitrogen is simpler than creating a sinusoidal wave. Concentration waves resulting from switching can be analysed by computing separate phase shifts for the different Fourier components of the wave. Finally, details of the practical data analysis are given and test results for oxygen diffusion in water are presented.

The diffusion coefficient and the diffusivity

Since diffusion and heat transport are closely related, it is useful to consider briefly the equation for one-dimensional heat transport.

$$C_h \frac{\partial T(x,t)}{\partial t} = \lambda \frac{\partial^2 T(x,t)}{\partial x^2}. \quad (1)$$

This equation shows that dynamic temperature patterns $T(x, t)$ depend on the ratio of the heat conductivity λ and the specific heat capacity C_h. This ratio has the dimension of a length squared per unit of time and is called the thermal diffusivity. For a sinusoidal temperature change at the soil surface, the solution of Equation (1) is well known (e.g. Hillel, 1980, pp. 303–308; Koorevaar *et al.*, 1983, pp. 195–198). In this paper the analogous solution for a sinusoidal concentration change is used.

Oxygen diffusion in unsaturated soil largely takes place through the gas-filled pores. Therefore, concentration gradients are usually expressed in terms of the concentration c_g in the gaseous phase (e.g. Currie, 1961; Rolston, 1986). Neglecting diffusion in the liquid phase, the diffusion equation becomes

$$\varepsilon \frac{\partial c_g(x,t)}{\partial t} = D \frac{\partial^2 c_g(x,t)}{\partial x^2}. \quad (2)$$

The heat capacity in Equation (1) is replaced by the gas-filled porosity, ε. The heat conductivity is replaced by the oxygen diffusion coefficient, D, which is often written as

$$D = D_0 \varepsilon f_g. \quad (3)$$

Here, D_0 is the diffusion coefficient in pure air and f_g is an impedance factor which accounts primarily of the tortuous pathway followed by the gas (cf. Nye & Tinker, 1977, pp. 76–83).

D can be measured for a core sample by means of a diffusion chamber in which the oxygen concentration c_g changes as a result of the diffusive flux through the sample (see Rolston, 1986; Bakker & Hidding, 1970). A dynamic concentration pattern in the soil, however, will not depend on D but on the ratio D/ε. This ratio is therefore defined as the

Table 1. Symbols, definitions and units.

Symbol	Description	Units	Equation
A_0	amplitude of sine wave at the surface	mol m^{-3}	(8)
$A_n(x)$	amplitude of nth component at depth x	mV	(16)
$a(x)$	relative amplitude at depth x	—	(11)
$a_n(x)$	sine part of nth Fourier component	mV	(14)
$b_n(x)$	cosine part of nth Fourier component	mV	(14)
β	gas solubility coefficient	—	(5, 6)
C_h	specific heat capacity	J m^{-3} K^{-1}	(11)
$c_g(x, t)$	concentration as function of x and t	mol m^{-3}	(9)
$c(x, t)$	electrode signal proportional to $c_g(x, t)$	mV	(13, 14)
c_{av}	average oxygen concentration	mol m^{-3}	(8)
D	diffusion coefficient of oxygen in soil	m^2 s^{-1}	(2)
D^*	oxygen diffusivity in soil	m^2 s^{-1}	(4, 6, 7)
D_0	diffusion coefficient in air	m^2 s^{-1}	(3)
D_w	diffusion coefficient in free water	m^2 s^{-1}	(5)
d	damping depth	m	(10)
ε	gas-filled porosity	m^3 m^{-3}	(2, 3, 4)
F	oxygen flux	mol m^{-2} s^{-1}	(5)
f_g	impedance factor for the gas-filled pores	—	(3, 4)
f_s	impedance factor at saturation	—	(5, 6)
λ	heat conductivity	W m^{-1} K^{-1}	(1)
θ_s	saturated water content	m^3 m^{-3}	(5, 6)
M	order of trend function	—	(14)
m	number of trend component (= 1, 2, 3, ...)	—	
N	number of Fourier components in fit	—	(14)
n	number of Fourier component (= 1, 2, 3, ...)	—	
$P_m(t)$	polynomial of order m	—	
$\varphi(x)$	phase shift at depth x	rad	(12)
$\varphi_n(x)$	phase shift relative to surface signal	rad	(18, 19)
$\varphi_n'(x)$	phase of nth component at depth x	rad	(15, 17)
t	time		
$T(x, t)$	temperature as function of x and t	K	(1)
ω	angular frequency	rad s^{-1}	
x	co-ordinate; distance to the surface	m	
$z_m(x)$	coefficient in mth trend component	mV	(14)

oxygen diffusivity D^*, given by

$$D^* = D/\varepsilon = D_0 f_g \tag{4}$$

for unsaturated soil.

In the limiting case of water saturation, the small contribution of diffusion in the liquid phase is predominant and the flux F becomes (cf. Nye & Tinker, 1977, pp. 83–86)

$$F = D\frac{\partial c_g(x,t)}{\partial x} = D_w\theta_s f_s \beta \frac{\partial c_g(x,t)}{\partial x}. \tag{5}$$

Note that the gradient is still written in terms of c_g, the gaseous concentration in equilibrium with the dissolved oxygen. The differential capacity for oxygen is now $\theta_s\beta$ and the relation between D^* and D becomes

$$D^* \equiv \frac{D}{\theta_s\beta} = D_w f_s \tag{6}$$

at saturation.

Equations (5) and (6) show that diffusion coefficients and oxygen fluxes are strongly affected by the low solubility β of oxygen in water (0.048 at 0°C, Nye & Tinker, 1977, pp. 83–86). The saturated diffusivity, however, is independent of the solubility.

A sinusoidal concentration wave

At the surface of a soil sample a sinusoidal concentration wave is applied. At a large depth, the concentration does not vary and approaches an average value c_{av}. The differential equation describing this is

$$\frac{\partial c_g(x,t)}{\partial t} = D^* \frac{\partial^2 c_g(x,t)}{\partial x^2} \tag{7}$$

with boundary conditions

$$\begin{aligned} c_g(x,t) &= c_{av} + A_0 \sin \omega t, \quad x = 0 \\ c_g(x,t) &\to c_{av} \qquad\qquad , \quad x \to \infty. \end{aligned} \tag{8}$$

The solution for the concentration $c_g(x,t)$ at time t at a distance x from the surface is

$$c_g(x,t) = c_{av} + A_0 \exp\left(\frac{-x}{d}\right)\sin\left(\omega t - \frac{x}{d}\right). \tag{9}$$

The concentration $c_g(x,t)$ at a depth x depends on a characteristic length d, the damping depth. This depth is determined by the diffusivity D^* and the angular frequency ω according to

$$d = \sqrt{2D^*/\omega}. \tag{10}$$

Equation (9) shows that the amplitude of the concentration wave decreases exponentially with depth. A relative amplitude $a(x)$ is defined as the ratio between the amplitude at a depth x and the amplitude A_0 at the surface. From Equation (9), it follows that

$$a(x) = \exp(-x/d). \tag{11}$$

The concentration wave at depth x also shows a phase shift $\varphi(x)$, a delay relative to the surface wave. The phase shift increases linearly with x according to

$$\varphi(x) = x/d. \tag{12}$$

The relative amplitude and the phase shift both depend only on the ratio x/d. Hence, the damping depth d can be determined by measuring either $a(x)$ or $\varphi(x)$. Once d is known, the diffusivity D^* is calculated using the (known) angular frequency and Equation (10).

In principle, the relative amplitude and the phase shift should both lead to the same damping depth. In practice, however, measured functions $a(x)$ and $\varphi(x)$ will not always be consistent. Two reasons for preferring the phase shift in such cases are discussed below.

The influence of macropores

The derivation above holds for a homogenous soil and a flat geometry. A more realistic situation is drawn in Fig. 1. The oxygen electrode penetrates into an aggregate from the surface. The electrode is 1 mm thick and amplitudes and phase shifts are measured at several depths between 0 and 4 mm, for instance. At small depths the diffusion is dominated by the presence of the flat surface of the cross section. The air-filled macropores are relatively distant from the electrode. At larger depths the situation changes. Air-filled macropores represent open channels to the surface and, when the electrode approaches a macropore, measured oxygen concentrations will certainly be influenced.

The problem is the extent to which the presence of macropores will influence the validity of Equations (11) and (12) near the surface. The presence of macropores implies that the assumption of a plane geometry does not hold. Some insight in the consequences was gained by studying the behaviour of concentration waves for non-plane geometries.

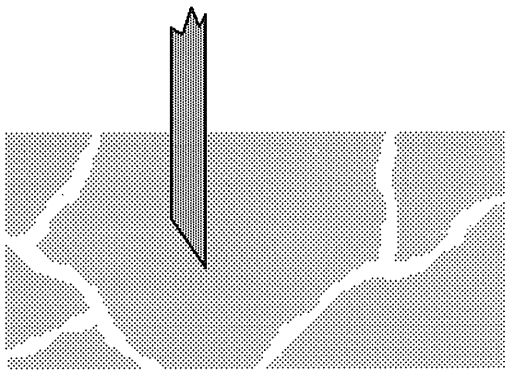

Fig. 1. An oxygen electrode penetrating the soil between air-filled macropores.

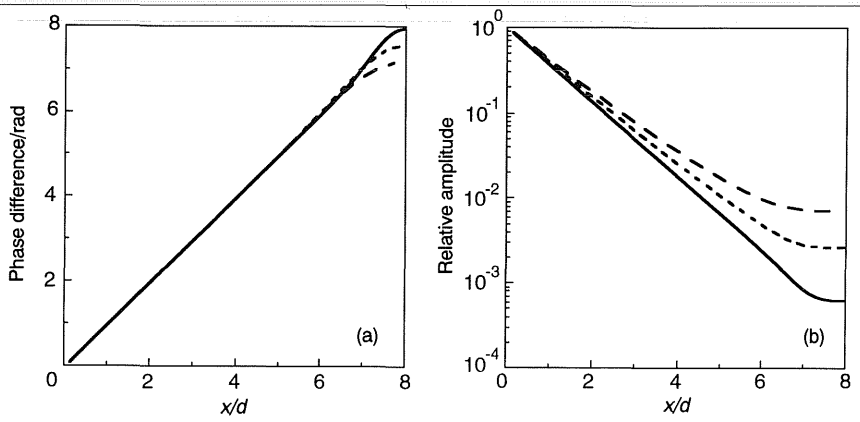

Fig. 2. Numerical calculations for a sinusoidal concentration wave applied to the surface of a plane, cylindrical or spherical soil aggregate with $R = 8d$. The concentration wave inside the aggregate has shifted in phase and has a reduced amplitude. (a) Except in the centre, the phase shift of the signal increases linearly with the distance x, independent of aggregate shape. (b) The decrease of the wave amplitude depends on aggregate shape. ——, Sheet; - - - -, cylinder; - - -, sphere.

For a sinusoidal concentration wave, the diffusion equation was solved numerically for a plane sheet with a thickness of $2R$, for a cylinder with radius R, and for a sphere with radius R. For these three object types the relative amplitude and phase shift were calculated as functions of the distance x to the outer surface. Figure 2 shows the results for R equal to 8 times the damping depth d. The graphs of $\varphi(x)$ in Fig. 2a are very similar for all three shapes. Near the surface, phase shifts are always accurately described by Equation (12). The results for the relative amplitude in Fig. 2b show, from the surface onwards, considerable differences between the different shapes.

These results are relevant for understanding the situation of Fig. 1. As long as the distance to the macropore system is larger than the distance to the surface, phase shifts will be given by Equation (12). The relative amplitude will be more sensitive to the presence of macropores. Consequently, a correct damping depth is more likely to be obtained from phase shifts than from relative amplitudes.

A second reason for preferring phase shifts is that they are independent of slow changes in the performance of the oxygen electrode. In fact, for measuring phase shifts, there is no need to calibrate the electrode. When amplitudes are measured, however, the calibration constant of the electrode must not change with depth.

Experimental details

A Polarografic electrode was used (Revsbach *et al.*, 1983). The platinum wire (with a sensing tip of approximately 50 μm) was protected against mechanical forces by sheathing it in stainless steel syringe needles, 10 cm long with a diameter of 1 mm. A polarization potential of −0.75 V was applied to the platinum. The platinum surface was not recessed relative to the needle surface. In order to decrease the oxygen consumption of the electrode, the platinum tip was covered with a membrane of cellulose nitrate. The membrane caused a significant reduction of the signal in water (by at least a factor of two). The oxygen electrode was pushed downward by attaching it to a small platform which was moved with a computer-controlled stepper motor.

The current caused by the reduction of oxygen was measured by means of an operational amplifier with a low input bias current in combination with a feedback resistor of 100 MΩ (= 1 mV output voltage for each 10 pA input current). The amplifier circuitry floats at the polarization potential, which was (electronically) subtracted from the mV signal. The result was further amplified using a d.c. amplifier, digitized, and made available to a computer. Due to a capacitor placed over the feedback resistor of 100 MΩ, the characteristic reaction time of the system was about 1 s. This led to a considerable noise reduction without being of any importance for measuring the much slower varying oxygen concentrations. A calomel electrode was used to close the electrical circuit.

The concentration wave was applied to the flat surface of a core sample. The core sample was placed in a container with holes for electrode entry (Fig. 3). A small gas flow was maintained through the container. By means of a relay-operated gas switch the computer could switch between nitrogen and air. The switching was carried out with a period

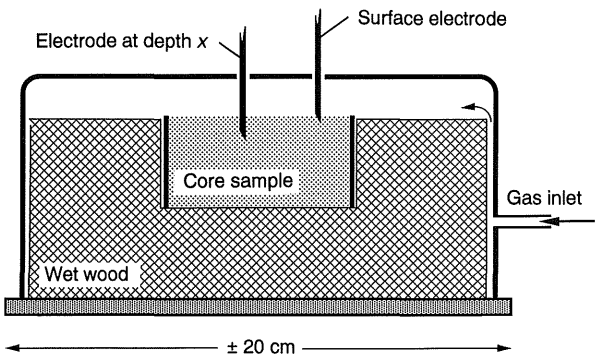

Fig. 3. A core sample placed in a box in which the oxygen concentration is periodically changed. Oxygen electrodes are placed in the soil and at the soil surface. The wet wood keeps the humidity high and reduces the box volume.

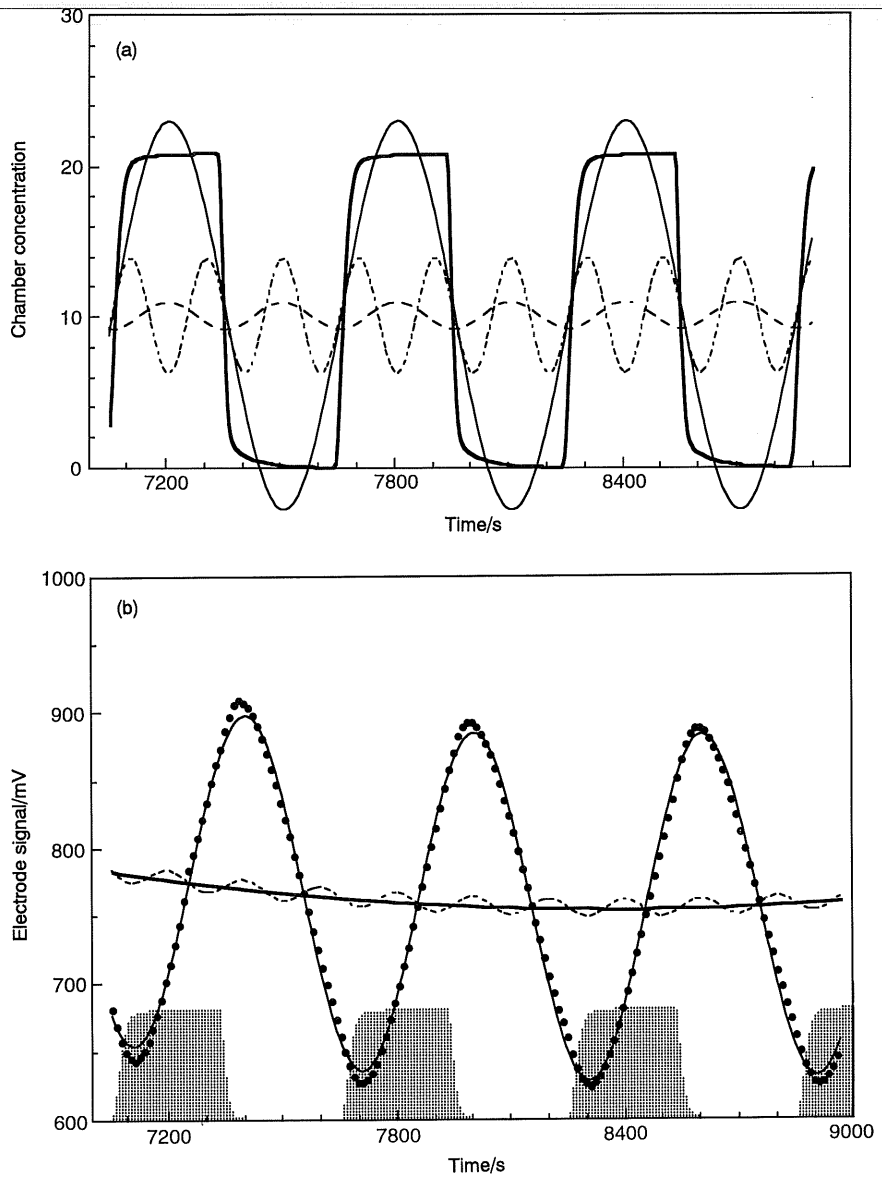

Fig. 4. Fourier analysis of the concentration wave at the surface and in the soil. (a) The surface signal with a period of 600 s and its first three Fourier components. ——, Surface electrode; harmonic components: —— $n=1$; – – –, $n=2$; - - - -, $n=3$. (b) The (uncalibrated) soil signal at almost two times the damping depth with its first and third Fourier component. ●, Sampled signal (mV); ——, second order trend; ——, trend + first harmonic; - - - -, trend + third harmonic; ▒, shape of surface wave.

of 600 s, which corresponds to an angular frequency of 0.01047 rad s^{-1}.

Concentration changes at a few times the damping depth are small compared to the average signal (cf. Fig. 2b). The periodicity of the signal and the known frequency greatly simplify the detection of the signal, however. With the electrodes and amplifiers used, sine waves have been detected which were 1000 times smaller than the surface wave. This corresponds to a depth of about 7 times the damping depth in the case of a plane geometry (cf. Fig. 2b and Equation 11).

Due to slow changes in the gas flow, the shape of the concentration wave at the surface could not be kept constant over many wave periods. Consequently, the surface concentration had to be measured continuously with a second oxygen electrode at the surface (see Fig. 3).

Data analysis

Switching between air and nitrogen does not lead to a concentration wave with a sinusoidal shape. The signal is still periodic, however, and may therefore be regarded as the sum of a number of sinusoidal components, the so-called harmonic or Fourier components of the signal. The angular frequencies of the Fourier components are $n\omega$ with $n=1,2,3,\ldots$. As the diffusion equation is a linear differential equation, the different harmonic components of the concentration wave can be treated independently of each other. The nth component leads to a damped oscillation at depth x with angular frequency $n\omega$. The signal measured at depth x is the sum of the concentration waves caused by the different harmonic components in the surface wave. Hence, by calculating the nth harmonic component of both the surface signal and the signal at depth

x, a phase shift can be determined belonging to an angular frequency $n\omega$. Figure 4 shows phase shifts calculated for the first, second and third harmonic component of signals measured at the surface (Fig. 4a) and at almost twice the damping depth (Fig. 4b).

The surface signal in Fig. 4a, and its first, second and third harmonic components, have been expressed as a concentration between 0% and 21% oxygen. After switching, it takes a few minutes before the surface concentration reaches 0% or 21%. Therefore, the surface concentration is not a symmetric square wave. Its decomposition into harmonic components is written as

$$c(0,t) = c_{\mathrm{av}} + \sum_{n=1}^{\infty} \underbrace{\{a_n(0)\sin n\omega t + b_n(0)\cos n\omega t\}}_{n\text{th harmonic component}}. \qquad (13)$$

The nth harmonic component is written as the sum of a sine and cosine function and c_{av} is the average concentration .

In principle, the electrode signal measured at any depth x can be analysed in the same way. Moving the electrode to a greater depth, however, caused a sharp and wholly unrealistic peak in its signal. This instability was probably caused by the mechanic force on the electrode. (During test measurements in water, there was hardly any instability.) After the sharp peak the signal stabilized, but a neat periodicity appeared only after one or two periods of 600 s. Waiting for a completely stable periodic signal would have taken too much time. Usually, the measurements were interrupted after 4 or 5 periods in order to change depth again. During the last 2 or 3 periods, the relatively stable signal still had a trend superimposed on it, as shown in Fig. 4b. The periodic part of the signal has to be separated from the trend, which is accomplished by writing the (uncalibrated) signal $c(x,t)$ at depth x as

$$c(x,t) = \underbrace{\sum_{m=0}^{M} z_m(x)P_m(t)}_{\text{trend function}} + \underbrace{\sum_{n=1}^{N}\{a_n(x)\sin n\omega t + b_n(x)\cos n\omega t\}}_{\text{periodic signal}}. \qquad (14)$$

The periodic part consists of N harmonic components written again as the sum of a sine and cosine term. In theory, the number of harmonic components is infinite, but in practice only a few of them can be calculated. The trend function is the sum of M polynomials $P_m(t)$ of order m. The simplest choice is $P_m(t) = t^m$, which makes the trend function a power series. When high-order trends are used, it is advantageous to use Legendre polynomials as trend functions $P_m(t)$.

The Fourier coefficients $a_n(x)$ and $b_n(x)$ of the signal at depth x and the M parameters $z_m(x)$ of the trend function were calculated using Equation (14) as a linear regression model. Chatfield (1975, p. 133) showed that the Fourier components of a signal are equal to the least squares estimates derived with a linear regression model with sine and cosine terms. It is assumed here that this remains approximately true when a simple trend function is added to the regression model. The advantages of the regression technique are that the inclusion of a trend function is straightforward and that the data points do not need to be equally spaced. It has the disadvantage of requiring more computing time than Fourier analysis. The least squares estimates of the $a_n(x)$, $b_n(x)$ and the trend parameters were found by means of singular value decomposition as described in Press *et al.* (1986).

Surface signals as in Fig. 4a were analysed by setting the order of the trend function, M, at zero (no trend) and the number of Fourier components, N, at 20. For describing the signals at depth x, fewer harmonic components are needed. The signal in Fig. 4b consists largely of its first harmonic component. This component has shifted 196 s to the right relative to the first harmonic in the surface signal, which means a phase shift of 2.05 rad or about a third period. In the signal in Fig. 4b a second and third harmonic component are just detectable, the latter being shown in the figure. The third harmonic has shifted 93 s compared to the third harmonic in Fig. 4a. With a period of 200 s (=600/3) this means a phase shift of 2.92 rad.

The amplitude of the third harmonic in the surface signal is about 300 per cent of the size of the first component. In Fig. 4b the third harmonic is much smaller since its three times larger frequency leads to a damping depth which is a factor $\sqrt{3}$ smaller (cf. Equation 10). At larger depths, the higher-order harmonic components disappear completely and only the sine wave of the first component remains. Figure 5 shows an example of this situation. The amplitude of the first harmonic component is about 300 times smaller than the average electrode signal (see the vertical axis). Clearly, it is only the periodic character of the signal which allows its separation from the relatively large trend and the noise. The concentration wave in Fig. 5 lies almost a full period (5.7 rad) behind the surface wave, which is drawn as hatched areas above the horizontal axis.

Some care is required in choosing the order M of the trend function. A 10th-order trend in Fig. 4b, for instance, would certainly describe also part of the periodic signal. In practice, M has been set at the smallest value consistent with a good fit. No attempt has been made to give this a precise mathematical meaning. Instead, graphs as Fig. 4b have been used to choose the smallest possible M by eye. A first- or second-order trend appeared to be sufficient in most cases.

In order to calculate phase shifts the nth-order harmonic in Equations (13) and (14) is written as a single sine function according to

$$n\text{th harmonic} = A_n(x)\sin[n\omega t - \varphi_n'(x)]. \qquad (15)$$

The total amplitude $A_n(x)$ of the nth harmonic at depth x is then calculated from the regression parameters $a_n(x)$ and $b_n(x)$ as

$$A_n(x) = \sqrt{a_n^2(x) + b_n^2(x)}. \qquad (16)$$

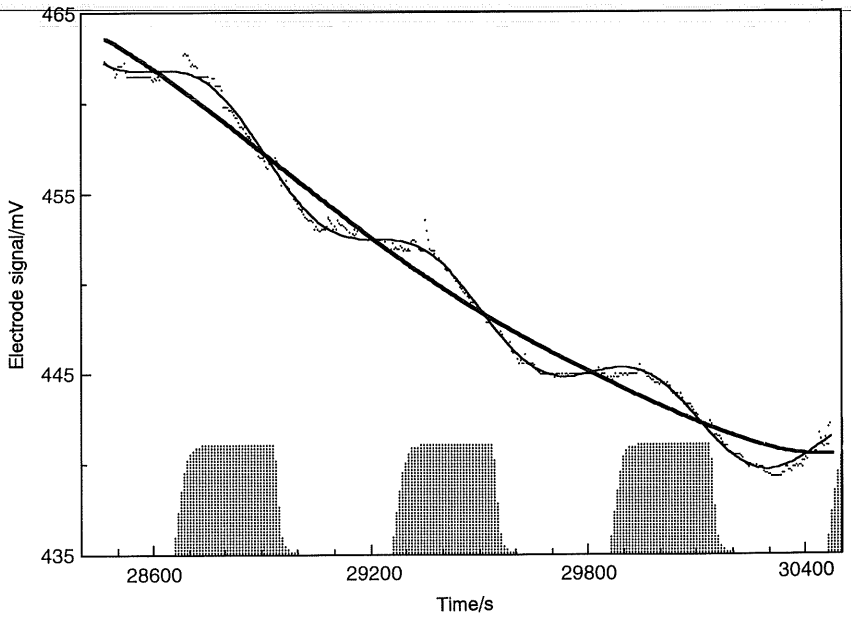

Fig. 5. At larger depths the concentration wave is smaller and sinusoidal, since the higher-order components have disappeared. A relatively large trend resulting from electrode instability is superimposed on the wave. The signal was analysed with linear regression analysis (cf. Equation 14). Sampled signal (mV); ——, sixth order trend; — —, fit with 1 harmonic term; ▩, shape of surface wave.

The phase $\varphi'_n(x)$ of the nth harmonic at $t=0$ is found by solving

$$\cos\varphi'_n(x) = +\frac{a_n(x)}{A_n(x)}$$
$$\sin\varphi'_n(x) = -\frac{b_n(x)}{A_n(x)}. \qquad (17)$$

The phase shift $\varphi_n(x)$ of the nth harmonic component relative to the surface signal is found now as the difference between the phases at depths 0 and x:

$$\varphi_n(x) = \varphi'_n(x) - \varphi'_n(0). \qquad (18)$$

By substituting an angular frequency $n\omega$ in Equations (10) and (12), the expected behaviour of $\phi_n(x)$ becomes

$$\varphi_n(x) = x\sqrt{n}/d \qquad (19)$$

in which d is the damping depth of the first harmonic. Hence, the ratio between the phase shift and $\sqrt{n}$ is equal to x/d for all harmonic components. This is to be used to calculate values of the damping depth d and the diffusivity D^*.

Testing the method

The electrode itself will disturb the concentration profile to some extent, both by its presence and by its oxygen use. For depths comparable to the needle diameter, deviations from a simple linear increase of the phase shift might be expected.

To get an impression of the importance of this effect, measurements were carried out in water with a small amount of agar added to it (0.5 g dm^{-3}). The agar prevents convective mixing. Figure 6 shows the measured phase shifts as a function of electrode depth. Phase shifts were calculated only for the first five harmonic components provided they were larger than a thousandth part of the surface signal. As a consequence of the shape of the applied surface wave, the first and third components were always the largest.

Figure 6 shows that the phase shifts start to increase from an offset depth of about 0.3 mm. The simple reason is that the actual electrode lies somewhat behind the needle tip. From the offset depth on, the increase is linear. No special behaviour at small depths could be observed. Apparently, the electrode does not significantly influence the concentration pattern, or at least the phase shift is robust against the changes induced by the electrode.

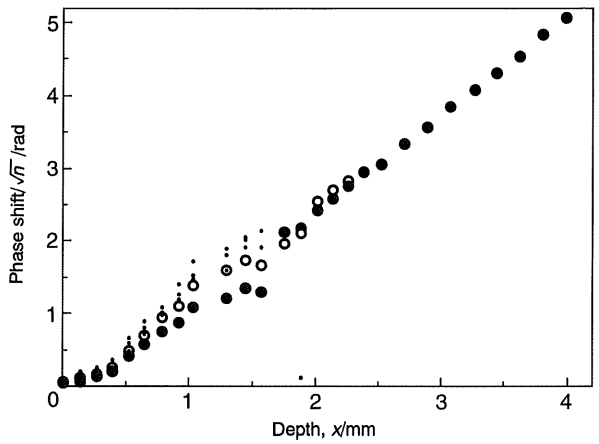

Fig. 6. Phase shifts measured in water with agar (0.5 g dm^{-3}). Results for different harmonic components have been combined in one graph by dividing the shifts by $\sqrt{n}$. The oxygen diffusivity derived from this graph is $(2.95 \times 0.06) \times 10^{-9}$ m^2 s^{-1}. ●, $n=1$; ○, $n=3$; •, $n=2, 4, 5$.

A straight line was fitted through the measured phase shifts for $n=1$ and $n=3$ (without using the data points for the lowest three depths, cf. Fig. 6). The resulting damping depth d is 0.750 ± 0.013 mm. Then, with a wave period of 600 s, Equation (10) gives a diffusivity of $(2.95 \pm 0.06) \times 10^{-9}$ m^2 s^{-1}. The water temperature was 23°C.

This result can be compared to values in the literature. Glinski & Stepniewski (1985) use 2.10×10^{-9} m^2 s^{-1} at 20°C and 2.38×10^{-9} m^2 s^{-1} at 25°C. Grable (1966) reports a larger value, 2.60×10^{-9} m^2 s^{-1} at 25°C. Hence, the value found in this paper is probably about 20% too large. No clear explanation could be found. Soil diffusivities, however, vary by several orders of magnitude and a systematic error of 20% does not prevent useful comparative measurements.

Results

Figure 7a shows the results of measurements in a core sample of clay soil with an air-filled porosity of 0.073 m^3 m^{-3}. Phase shifts were calculated for harmonic components larger than a thousandth part of the surface signal. The regression was based on the phase shifts for $n=1$ and $n=3$ at the first four depths and corresponds to a diffusivity of $(0.81 \pm 0.06) \times 10^{-9}$ m^2 s^{-1}. The offset depth for the measurements in soil was 0.89 mm. Using that value, the measurements shown in Fig. 7b can be interpreted consistently (the same electrode was used). The line in that figure leads to a diffusivity of $(0.96 \pm 0.11) \times 10^{-9}$ m^2 s^{-1}. The deviations for $x=1.2$ mm and $x=1.5$ mm may have been caused by leakage along the electrode (for larger depths this leakage was prevented by the grease applied to the electrode needle). The air-filled porosity of the second core sample was 0.038 m^3 m^{-3}.

In both graphs of Fig. 4, the measured phase shifts stop increasing at 2 or 3 mm from the surface. This probably reflects the influence of air-filled pores (cf. Fig. 1). The observed distance of a few mm indicates the size of the saturated zones between the air-filled pores.

For entire core samples, macroscopic diffusion coefficients were measured using a diffusion chamber as described by Bakker & Hidding (1970) and Rolston (1986). For 10 soil samples with air-filled porosities between 0.02 and 0.07 m^3 m^{-3}, the measured macroscopic diffusion coefficients varied between 13×10^{-9} m^2 s^{-1} and 310×10^{-9} m^2 s^{-1} with an average value of 75×10^{-9} m^2 s^{-1}.

Discussion

A diffusion coefficient measured with a diffusion chamber is the ratio between a flux and a concentration gradient. The diffusivity measured by observing concentration changes in the soil is a different quantity and some care is required in calculating one from the other. The ratio between the two is the differential capacity of the soil for oxygen, which is approximately ε for unsaturated soil and $\theta_s \beta$ for saturated soil (cf. Equations 4 and 6).

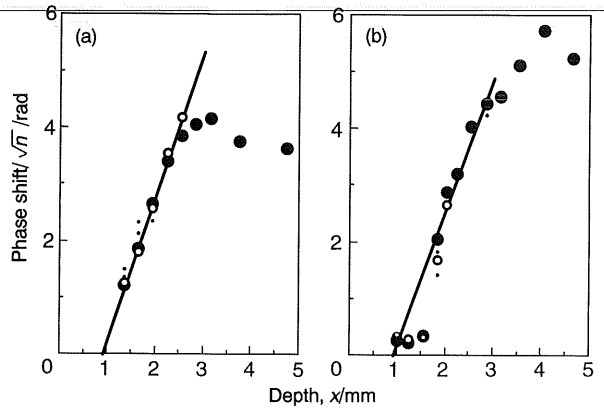

Fig. 7. Phase shifts for different harmonic components measured in soil. The two regression lines have a common offset depth of 0.89 mm and lead to diffusivities of (a) 0.81×10^{-9} m^2 s^{-1} and (b) 0.96×10^{-9} m^2 s^{-1}. ●, $n=1$; ○, $n=3$; •=2, 4, 5.

The diffusivity of about 0.9×10^{-9} m^2 s^{-1} measured with the oxygen electrodes on a millimetre scale is an extremely low value for unsaturated soil. In fact, it is lower than the diffusion coefficient D_w of oxygen in pure water (2.10×10^{-9} m^2 s^{-1}; Glinski & Stepniewski, 1985). This is understood by assuming local saturation of the soil with water. Equation (6) may then be used to calculate the impedance factor f_s for the saturated spot. The result is 0.43, which is a realistic value. Nye & Tinker (1977, pp. 75–86) mention that values between 0.4 and 0.7 have been obtained for diffusion in saturated soil.

The measured diffusivity D^* can be used to estimate a value for the local diffusion coefficient. With Equation (6), a saturated water content of about 0.4 m^3 m^{-3} and an oxygen solubility β of about 0.03, the diffusion coefficient for soil, D, becomes 0.012×10^{-9} m^2 s^{-1}, which is about 6000 times smaller than the average diffusion coefficient of 75×10^{-9} m^2 s^{-1} measured for the entire soil cores.

For the clay soil used the extent of the small saturated zones between air-filled pores is a few millimetres. In combination with a diffusion coefficient as low as the estimated value above, this may well lead to anaerobiosis between individual air-filled pores. In general, the importance of small saturated zones will depend on the size of these zones compared with the distance characterizing the transport process studied, the penetration distance for oxygen, for instance. Hence, an important characteristic of soil structure is the geometry of the air-filled part of the pore system as a function of the water content.

In principle, an oxygen electrode may also be used to measure the diffusivity at larger scales. The electrode then passes air-filled pores and the phase shift will fluctuate. The average phase shift, however, will increase slowly expressing a macroscopic diffusivity. Whether or not this diffusivity is the same as the diffusivity for a whole core sample is unknown; the electrodes used were too fragile to be driven into the clay soil more than a few millimetres.

Acknowledgements

I thank J. Beukema and H. van Gemerden of the microbiology department in Groningen for constructing the oxygen electrodes. The apparature for moving the electrode was build by T. Erenst, L. Herben, J. van de Goor and E. Janssen. The core-sample diffusion coefficients were measured by B. Kroesbergen. Finally, I thank J.H.G. Verhagen, P.A. Leffelaar and P.A.C. Raats, the late Professor C.T. de Wit and the two referees for their help and their comments on the manuscript. The work was supported by the Netherlands Integrated Soil Research Program.

References

Bakker, J.W. & Hiding, A.P. 1970. The influence of soil structure and air content on gas diffusion in soils. *Netherlands Journal of Agricultural Science,* **18,** 37–48.

Chatfield, C. 1975. *The Analysis of Time Series: An Introduction.* Chapman and Hall, London.

Currie, J.A. 1961. Gaseous diffusion in aeration of aggregated soils. *Soil Science,* **92,** 40–45.

Glinski, J. & Stepniewski, W. 1985. *Soil Aeration and its Role for Plants.* CRC Press, Boca Raton, FL.

Grable, A.R. 1966. Soil aeration and plant growth. *Advances in Agronomy,* **18,** 57–106.

Hillel, D. 1980. *Fundamentals of Soil Physics.* Academic Press, New York.

Koorevaar, P., Menelik, G. & Dirksen, C. 1983. *Elements of Soil Physics.* Elsevier, Amsterdam.

Nye, P.H. & Tinker, P.B. 1977. *Solute Movement in the Soil–Root System.* Blackwell Scientific Publications, Oxford.

Press, W.H., Flannery, B.P., Teukolsky, S.A. & Vetterling, W.T. 1986. *Numerical Recipes, the Art of Scientific Computing.* Cambridge University Press.

Revsbech, N.P., Jørgensen, B.B., Blackburn, T.H. & Cohen, Y. 1983. Micro-electrode studies of the photosynthesis and O_2, H_2O and pH profiles of a microbial mat. *Limnology and Oceanography,* **28,** 1062–1074.

Rolston, D.E. 1986. Gas diffusivity. In: *Methods of Soil Analysis: Part 1, Physical and Mineralogical Methods*, 2nd edn (ed. A. Klute), pp. 1089–1102. American Society of Agronomy, Madison, WI.